Subsurface oxygen and surface oxide formation at Ag(111): A density-functional theory investigation

Wei-Xue Li,[1,*] Catherine Stampfl,[1,2] and Matthias Scheffler[1]
[1]*Fritz-Haber-Institut der Max-Planck-Gesellschaft, Faradayweg 4-6, D-14195 Berlin-Dahlem, Germany*
[2]*Department of Physics and Astronomy, Northwestern University, Evanston, Illinois 60208*
(Received 11 August 2002; published 29 January 2003)

To help provide insight into the remarkable catalytic behavior of the oxygen/silver system for heterogeneous oxidation reactions, purely subsurface oxygen, and structures involving both on-surface and subsurface oxygen, as well as oxidelike structures at the Ag(111) surface have been studied for a wide range of coverages and adsorption sites using density-functional theory. Adsorption on the surface in fcc sites is energetically favorable for low coverages, while for higher coverage a thin surface-oxide structure is energetically favorable. This structure has been proposed to correspond to the experimentally observed (4×4) phase. With increasing O concentrations, thicker oxidelike structures resembling compressed $Ag_2O(111)$ surfaces are energetically favored. Due to the relatively low thermal stability of these structures, and the very low sticking probability of O_2 at Ag(111), their formation and observation may require the use of atomic oxygen (or ozone, O_3) and low temperatures. We also investigate the diffusion of O into the subsurface region at low coverage (0.11 ML), and the effect of surface Ag vacancies in the adsorption of atomic oxygen and ozonelike species. The present studies, together with our earlier investigations of on-surface and surface-substitutional adsorption, provide a comprehensive picture of the behavior and chemical nature of the interaction of oxygen and Ag(111), as well as of the initial stages of oxide formation.

DOI: 10.1103/PhysRevB.67.045408 PACS number(s): 81.65.Mq, 82.65.+r, 68.43.−h

I. INTRODUCTION

Investigation of the interaction of oxygen and silver, with regard to the role it plays in technologically important heterogeneous catalytic reactions such as ethylene epoxidation and the partial oxidization of methanol to formaldehyde, has a long history.[1] Despite considerable efforts, the O/Ag system is still not well understood on a microscopic level, and the identification of active oxygen species involved in the above-mentioned reactions, remains unclear. Of particular interest is to understand the role and nature of the elusive subsurface O species in the function of silver as an oxidation catalyst. Subsurface oxygen is thought to play a crucial role in the epoxidation of ethylene (i.e., formation of ethylene oxide, alternatively known as epoxide), which takes place under atmospheric pressure and temperatures of 500–600 K, and in the formation of formaldehyde from methanol, which can occur either by direct dehydrogenation or by oxidehydrogenation, and also takes place under atmospheric pressure and temperatures of 700–900 K and 800–900 K, respectively.[2–12]

Recent studies of oxidation reactions over certain other metal surfaces have found that metal oxides form and activate the reaction, in contrast to the hitherto believed pure metal, i.e., for the oxidation of carbon monoxide over Ru.[13,14] One may therefore wonder if similarly silver oxides form and play an important role. The most stable oxide of silver, Ag_2O, however, reportedly thermally decomposes at 460 K and at atmospheric pressure, making this seem unlikely; ruthenium dioxide on the other hand is stable up to temperatures greater than 1000 K.[15] To date there have been a limited number of *ab initio* studies of subsurface oxygen adsorption and oxide formation at transition-metal surfaces. These include the investigation of oxygen incorporation into the Ru(0001) surface[16,17] which predicted that after 1 ML of oxygen on the surface, O adsorbed in subsurface sites below the first Ru layer where an attractive interaction between the oxygen atoms was identified, suggesting island formation. Within these structures, the overall O-Ru bondstrength was reported to be significantly weaker than pure on-surface adsorption, thus representing a significant destabilization of the surface. Subsequent investigations of this system in more detail indicated that structures involving on-surface and subsurface oxygen functioned as nucleation sites and metastable precursor structures for bulk oxide formation and an atomic pathway for the transition to RuO_2 was predicted.[18] Similar studies for O/Rh(111)[19] have also recently been reported, as well as studies of the initial oxidation of alloy surfaces, i.e., NiAl(110).[20] From a recent trend study of oxygen adsorption and incorporation at the basal planes of Ru, Rh, Pd, and Ag, it was found that the coverage at which the onset of oxygen occupation of subsurface sites occurs, correlates closely with that predicted at which bulk oxide formation begins, and that this occurs at progressively lower coverages for the metals more to the right in the periodic table.[21] The energy cost for lattice distortion was found to play a key role, where it is greater for the metals more to the left in the periodic table (i.e., Ru and Rh). With regard to pure free-electron-like metals, the O/Al(111)[22] and O/Mg(0001)[23] systems have been investigated as well by first-principles calculations. Earlier studies using an embedded atom-type approach, focussed on the energy barriers for O penetration through the surface layer of various metals and oxides, which is an important consideration particularly with regard to the kinetics.[24] Our present investigation into the interaction of oxygen and Ag(111), in addition to sheding light on the understanding of how silver functions as an efficient oxidation catalyst, also

addresses the initial stages of oxide formation. Our general findings could have implications for gold, also a noble metal oxidation catalyst[25] which, for the (111) surface, exhibits a restructuring and chemisorption of oxygen atoms at elevated temperatures (500–800 K) and at atmospheric pressure,[26,27] very similar to Ag(111). The findings of the present study could also have consequences for copper, which catalyses the oxidation of methanol to formaldehyde.[28]

Experimental evidence indicates that the (111) orientation is an important crystal face for real silver catalysts since at high temperatures, facets with this face result[11,12] presumably due to the fact that it has the lowest surface energy. There are only two ordered phases of oxygen on Ag(111) that have been reported; the (4×4)[29] and $(\sqrt{3}\times\sqrt{3})R30°$ structures.[9,11] The latter actually exhibits a superstructure given in matrix notation as $(26\times1;-1\times26)$. The (4×4) structure has recently been investigated by scanning tunneling microscopy (STM) where the atomic structure is proposed to involve a thin surface-oxide layer.[30,31] In this work (Ref. 31), it was furthermore proposed that at low coverage ($\theta=0.05\pm0.03$ ML), O atoms occupied subsurface octahedral sites below the first Ag layer. As will be shown in our present work, however, on-surface adsorption at low coverage is significantly more favorable.

The $(\sqrt{3}\times\sqrt{3})R30°$ phase has also been investigated by STM, as well as by reflection electron microscopy and reflection high-energy electron diffraction. It forms only after the exposure of silver (irrespective of the crystal face) to O_2 at atmospheric pressure and high temperatures (800–900 K).[9,11] Various atomic structures have been proposed for this phase; our recent STM simulation supported a surface-substitutional geometry, however, it was noted that this structure was only *metastable*.[32] To date, the atomic geometry of neither of these ordered phases has been unambiguously confirmed which calls for further quantitative structural analyses.

In our previous work,[32] we studied both on-surface oxygen and oxygen adsorption in surface-substitutional sites on Ag(111) for a wide range of coverages. The bondstrength of on-surface oxygen was found to be weak compared to the transition metals to the left of silver in the periodic table (e.g. Ru). With increasing coverage, there is a strong repulsion between on-surface oxygen atoms, and the on-surface oxygen adsorption becomes energetically unstable with respect to gas phase molecular oxygen for coverages greater than $\simeq0.5$ ML. In the present paper, we investigate pure subsurface oxygen and structures involving both oxygen adsorbed on the surface and in the subsurface region, hereafter denoted as ''on-surface+subsurface.'' We also investigate the proposed (4×4) surface-oxide phase, and oxidelike structures containing higher oxygen concentrations. These results, together with our earlier study, provide a comprehensive understanding of the electronic and atomic structure, and stability of oxygen species at the Ag(111) surface.

The paper is organized as follows: The calculation method is briefly explained in Sec. II and in Sec. III, results are presented for purely subsurface O structures (i.e., without on-surface oxygen) where the energetics, atomic geometry, and electronic properties for different sites and for a wide range of coverages are described. Also energy barriers for oxygen penetration into the sub-surface region are reported. In Sec. IV structures are considered that involve both on-surface and subsurface oxygen species, as well as the earlier proposed (4×4) geometry.[30] In Sec. V, geometries involving higher concentrations of oxygen are considered, where the energetic preference of oxidelike structures is found which have a geometry similar to the (111) surface of Ag_2O. In this section, we also investigate an ozone-like species adsorbed at an Ag vacancy, as has been proposed to be the active species for ethylene epoxidation. The conclusions are given in Sec. VI.

II. CALCULATION METHOD

The density-functional theory (DFT) total-energy calculations are performed using the pseudopotential plane-wave method[33] within the generalized gradient approximation for the exchange-correlation functional.[34,35] The pseudopotentials are generated by the scheme of Troullier and Martins with the same functional.[36,37] The wave-functions are expanded in plane waves with an energy cutoff of 50 Ry and the surface is modeled by a five layer slab separated by 15 Å of vacuum. Oxygen is placed on one side of the slab where the induced dipole moment is taken into account by applying a dipole correction.[38] The positions of the oxygen atoms and the top three silver layers are relaxed until the forces on the atoms are less than 0.015 eV/Å. In the (1×1) Ag(111) surface unit cell, 21 special **k** points are used in the surface irreducible Brillouin zone for the Brillouin-zone integration.[39] These **k** points are equivalent for all of the surface structures studied in order to maximize the accuracy when comparing the energies of different coverages as calculated in different supercells. We employ a Fermi function with a temperature broadening parameter of $k_BT^{\mathrm{el}}=0.1$ eV, and the total energy is extrapolated back to zero temperature. (k_B is the Boltzmann constant.) Results of detailed convergence tests can be found in Ref. 32.

The average adsorption energy per oxygen atom, E_{ad}, is calculated according to

$$E_{\mathrm{ad}}=-\frac{1}{N_{\mathrm{O}}}[E^{\mathrm{O/Ag(111)}}-(E^{\mathrm{Ag(111)}}+N_{\mathrm{O}}E^{\mathrm{free\text{-}O}})], \qquad (1)$$

where N_{O} is the total number of oxygen atoms of the adsorbate-substrate system per unit cell, and the total energy of the adsorbate-substrate system, the clean surface, and the free oxygen atom are represented by $E^{\mathrm{O/Ag(111)}}$, $E^{\mathrm{Ag(111)}}$, and $E^{\mathrm{free\text{-}O}}$, respectively. That is, $E^{\mathrm{O/Ag(111)}}$ represents the O/Ag system under investigation, which, e.g., may involve purely subsurface O, or on-surface and subsurface species, or oxidelike structures.

To study the interaction between on-surface and subsurface oxygen, we consider how the stability of on-surface O is affected by subsurface O (and vice versa). To do this, we define a so-called ''removal energy,'' which is the energy required to remove an on-surface O atom into the vacuum. It is given as

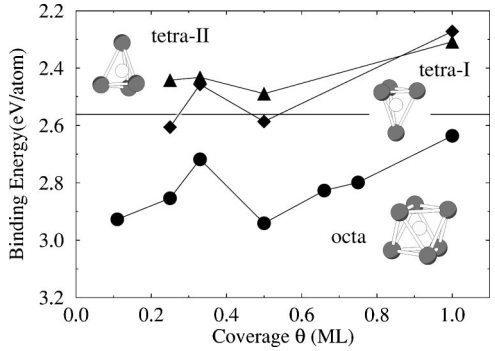

FIG. 1. Calculated adsorption binding energy of oxygen (with respect to atomic oxygen) under the first Ag(111) layer in octa (circles), tetra-I (diamonds), and tetra-II (triangles) sites, as a function of coverage. The horizontal full line represents half the experimental value of the binding energy of O_2 (2.56 eV). The solid lines connecting the calculated adsorption energies are to guide the eye.

$$E_{\mathrm{on}}^{\mathrm{removal}} = -[E^{\mathrm{O/Ag(111)}} - (E^{\mathrm{O_{sub}/Ag(111)}} + E^{\mathrm{free\text{-}O}})], \quad (2)$$

where $E^{\mathrm{O_{sub}/Ag(111)}}$ is the total energy of the ''reference'' system, i.e., that containing only (one or more) subsurface O species. $E_{\mathrm{on}}^{\mathrm{removal}}$ can also be thought of as the adsorption energy of an O atom onto the substrate which contains the subsurface O atoms. An obvious analogous equation holds for the removal energy of a subsurface O atom

$$E_{\mathrm{sub}}^{\mathrm{removal}} = -[E^{\mathrm{O/Ag(111)}} - (E^{\mathrm{O_{on}/Ag(111)}} + E^{\mathrm{free\text{-}O}})], \quad (3)$$

where $E^{\mathrm{O_{on}/Ag(111)}}$ is the total energy of the reference system, i.e., that containing only the on-surface O species. We consider $E_{\mathrm{sub}}^{\mathrm{removal}}$ only for structures having one O atom on the surface and one below it. The adsorption and removal energies are defined such that a positive number indicates that the adsorption is exothermic (stable) with respect to a free O atom, and a negative number, endothermic (unstable).

The definitions of quantities that we use to analyze our results, e.g., total and projected density of states (PDOS), density difference distributions, and the work function, can be found in Refs. 40,32.

III. PURE SUB-SURFACE OXYGEN

We first study the subsurface oxygen without the presence of on-surface oxygen. For oxygen occupation in the subsurface region there are two possible sites: (i) the octahedral site, denoted hereafter as ''octa,'' which has six nearest-neighbor Ag atoms, three above and three below, and (ii) the tetrahedral site, which has four nearest-neighbor Ag atoms. Due to the presence of the surface, there are two types of tetrahedral sites; one is where there are three silver atoms above it and one below, denoted as tetra I, and the alternative one, tetra II, is just the opposite with one surface Ag atom directly above, and three below it in the second Ag layer, as depicted in the insets of Fig. 1. We performed calculations for oxygen in these different sites for a wide range of coverages, i.e., 0.11 to 1 ML. We focus on adsorption immediately below the first Ag layer as we find that oxygen adsorption deeper in the bulk is less favorable in every case (see Table I). In the following subsections, the energetics, the atomic and electronic structures, and energy barriers for O diffusion into the substrate are discussed, respectively.

TABLE I. Calculated energies (in eV) and first metal interlayer expansion for various coverages of subsurface oxygen in the octa, tetra-I, and tetra-II sites. E_{ad} is the adsorption energy with respect to atomic oxygen and E_{b} is the binding energy on the predistorted surface, and E_{d} is the energy cost of the distortion of the substrate as induced by subsurface oxygen (without the presence of O, see text). Δd_{12} is the percentage change in the first metal interlayer distance, where the center of mass of each layer is used. The calculated bulk interlayer distance is 2.43 Å. Where available, values of the adsorption energy are given for O occupation under the second metal layer, E_{ad}(second).

θ(ML)		0.11	0.25	0.33	0.50	0.66	0.75	1.00
Octa								
	E_{ad}	2.93	2.86	2.72	2.94	2.83	2.80	2.64
	E_{b}		3.40	3.16	3.40		3.15	2.91
	E_{d}		0.54	0.44	0.46		0.35	0.27
	Δd_{12}	6.4	10.9	10.5	21.2	28.6	29.9	33.2
	E_{ad}(second)	2.72	2.64	2.70				
Tetra I								
	E_{ad}		2.61	2.46	2.59		2.45	2.27
	E_{b}		3.49	3.14	3.32		2.97	2.65
	E_{d}		0.88	0.68	0.73		0.52	0.38
	Δd_{12}		15.5	14.2	27.4		41.1	46.8
	E_{ad}(second)	2.31	2.19					
Tetra II								
	E_{ad}		2.44	2.43	2.49			2.31
	Δd_{12}		17.5	20.4	37.3			49.2

A. Energetics

The calculated adsorption energies E_{ad} for O_{octa}, $O_{tetra\text{-}I}$, and $O_{tetra\text{-}II}$, with respect to atomic oxygen, are plotted in Fig. 1 and are listed in Table I. For O_{octa} (circles), it can be seen that the adsorption energy decreases when the coverage varies from 0.11 to 0.33 ML, indicating a repulsive interaction between the O_{octa} atoms; however, it increases from 0.33 to 0.50 ML, so that the effective interaction between the O_{octa} atoms in this range is attractive. For coverages higher than 0.50 ML, the adsorption energy decreases again. Despite this dependence on coverage, we note that the overall variation in the magnitude of the adsorption energy is rather small, i.e., not greater than 0.3 eV—in sharp contrast to what we found for adsorption on the surface, where the corresponding value is 1.93 eV.[32] Compared to O_{octa}, the tetrahedral sites are energetically less favorable for the whole coverage range. It can be noticed that the tetrahedral sites exhibit a similar dependence on coverage as O_{octa}.

From our calculations, the *relative stability* of the various systems are well defined; the absolute value of the adsorption energies is less so due to the error of standard DFT calculations in describing the free O atom and molecule.[32] In particular, the experimental binding energy of O_2 per O atom is 2.56 eV while the calculated value is 3.16 eV/atom,[32] that is, the theoretical value is significantly overestimated. The deviation to the experimental value highlights the difficulty in obtaining quantitatively, the absolute adsorption energies. This is particularly problematic for this system as can be appreciated from Fig. 1: On the consideration of the theoretical value of 3.16 eV, it would indicate that all of the subsurface sites are unstable with respect to the oxygen molecule, while the experimental value indicates that the octa site is stable with respect to O_2 for all the coverage range. The adsorption energy of oxygen on the substrate is expected also to be overbound, although not nearly so severely as the O_2 molecule.

Compared to subsurface adsorption, on-surface adsorption is notably more favorable for low coverages: compare 3.61 eV[32] (fcc) to 2.93 eV (octa, Table. I) for coverage 0.11 ML and 3.52 eV[32] (fcc) to 2.86 eV (octa, Table I) for coverage 0.25 ML. Due to the build-up of a strong repulsion between on-surface adsorbates,[32] for a coverage of 0.50 ML, the energies of on-surface and sub-surface oxygen become practically degenerate [compare 2.92 eV[32] (fcc) and 2.94 eV (octa, Table I)]. For higher coverages, on-surface adsorption becomes considerably less favorable than subsurface oxygen.

The electron density at subsurface sites is significantly greater than for on-surface sites which gives rise to a strong kinetic repulsion due to the orthogonalization of the wavefunctions of the substrate caused by the presence of oxygen. To reduce this repulsion, the lattice expands to an optimum value.[41] In order to aid our discussions concerning on-surface versus subsurface adsorption, it is constructive to regard the subsurface adsorption energy, E_{ad}, as consisting of two contributions: (i) the energy cost of distorting the (clean) substrate lattice to the geometry induced by subsurface oxygen E_d and (ii) the binding energy of oxygen on the predistorted substrate, E_b, i.e., $E_{ad}=E_b-E_d$. We may then regard the binding energy as being due only to electronic effects, as we have removed the energy cost of distorting the lattice; that is, as purely reflecting the bond strength of the O-Ag interaction. We have calculated these contributions for the octa and tetra I sites which are given in Table I and are also plotted in Fig. 2, along with the corresponding on-surface adsorption energies[32] for comparison. In addition, the percentage change in the first metal-metal interlayer distance is shown.

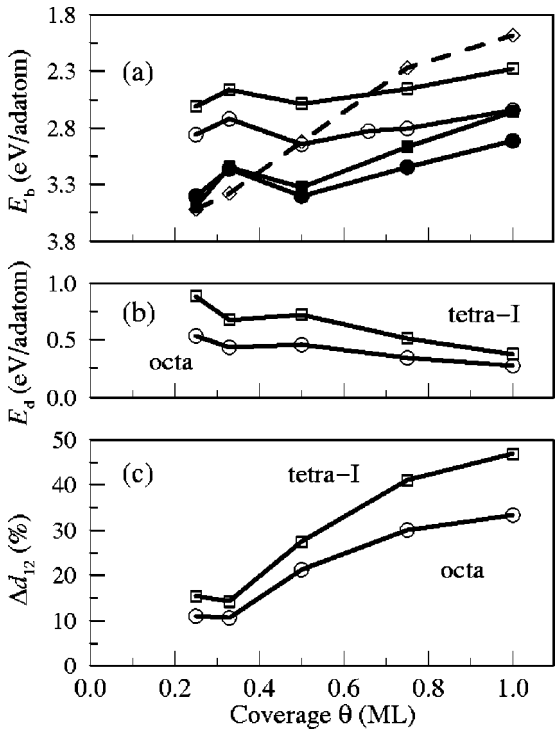

FIG. 2. (a) Binding energies of O on the predistorted substrate, E_b, in the octa (filled circles) and tetra-I sites (filled squares) and the corresponding adsorption energies E_{ad} of O in the octa (open circles) and tetra-I (open squares) sites. The adsorption energies of on-surface fcc-O are also shown (open diamonds). (b) Energy cost E_d of distorting the substrate lattice to the geometry induced by subsurface oxygen (but without the presence of oxygen) for the octa (open circles) and tetra-I (open squares) sites. (c) Percentage change of the first metal interlayer distance compared to the bulk value for the octa (circles) and tetra-I (squares) sites.

Comparing the binding energies of O on the predistorted surface with on-surface adsorption [see Fig. 2(a)], it can be seen that for coverages 0.25 and 0.33 ML, on-surface adsorption is still (slightly) energetically more favorable than subsurface adsorption in either the octa or tetra-I sites, thus the preference for O to be on the surface is not due to the energy cost of distortion of the substrate for the case of subsurface adsorption. It can be seen, however [from e.g., Fig. 2(b)] that the energy cost of distortion is significant and does reduce the adsorption energy of subsurface oxygen substantially. For example, at 0.50 ML the binding energy of subsurface oxygen in the octa site on the predistorted substrate is 0.48 eV greater than adsorption on the surface, but the *adsorption* energy (i.e., when paying for the distortion cost) is practically the same. Furthermore, it can be seen that like the ad-

sorption energy, only to a greater degree, the binding energy of subsurface oxygen decreases in the coverage range 0.50–1.0 ML. This repulsive interaction is attributed to unfavorable O-O interactions due to the close proximity of the partially negatively charged O atoms to one another and the larger expansion of the metal-metal spacing for these coverages, which less effectively screens the O atoms.

The energy cost of distorting the substrate [Fig. 2(b)] per O atom generally decreases with increasing O coverage due to an effective sharing of the energy cost by neighboring O atoms. The exception, from coverage 0.33 to 0.50 ML, where the distortion energy slightly increases, is because there is a significant increase of the metal interlayer spacing for the latter coverage [see Fig. 2(c)]. The distortion energy is always larger for the tetra-I site, which is understandable due to the larger oxygen-induced expansion of the first metal interlayer spacing [see Table I and Fig. 2(c)] caused by the smaller space in which to accommodate the subsurface O atom.

As seen clearly from Fig. 1, the adsorption energy for the octa site is greater than the tetrahedral sites for all the coverages considered. If we remove, however, the distortion energy, we see from Table I [and Fig. 2(a)] that for coverage 0.25 ML, the tetra-I site has in fact slightly greater binding energy (compare 3.49 to 3.40 eV). In this case it is the larger cost of distortion for the tetra-I site (compare 0.88 to 0.54 eV) that results in the octa site having the larger adsorption energy. For all the higher coverages, however, the octa site has the stronger O-Ag binding and even though the energy cost of distortion for the tetra-I site is larger than the octa site in all cases, this does not determine the adsorption site preference and make the tetra-I site less favorable than the octa site. The reason that the binding energy of the tetra-I site is less favorable than the octa site for coverages greater than 0.25 ML, is therefore an electronic effect. This could be due to a less efficient screening by the metal atoms of the partially negatively charged subsurface O atoms, due to the larger Ag-Ag interlayer spacing of the tetra-I site as shown clearly in Fig. 2(c).

The above findings highlight the interplay between the energy gain due to bond formation and the energy cost due to structural deformation. These effects are materials dependent: To the left of Ag in the periodic table, the transition metals are ''harder'' (i.e., having higher bulk moduli), and the energy cost of deformation is higher;[21] on the other hand, the energy gain due to bond formation between oxygen and the transition metal is stronger as well.

B. Atomic structure and electronic properties

As seen above, subsurface oxygen occupation induces a significant structural distortion of the Ag(111) substrate as shown by the variation of the first interlayer spacing in Table I and in Fig. 2(c): Namely, the expansion varies from 0.16 to 0.81 Å for O_{octa} when θ increases from 0.11 to 1.00 ML, and from 0.38 to 1.14 Å for $O_{tetra\text{-}I}$, and from 0.43 to 1.20 Å for $O_{tetra\text{-}II}$, when θ increases from 0.25 to 1.00 ML. This is in sharp contrast to what we found in our study of on-surface oxygen adsorption where the contraction of the first interlayer spacing induced by on-surface oxygen was less than 0.02 Å for the whole coverage range investigated (0.11 to 1.00 ML).[32] The large expansion is, however, similar to what has been found for subsurface O at other metal surfaces.[17,18]

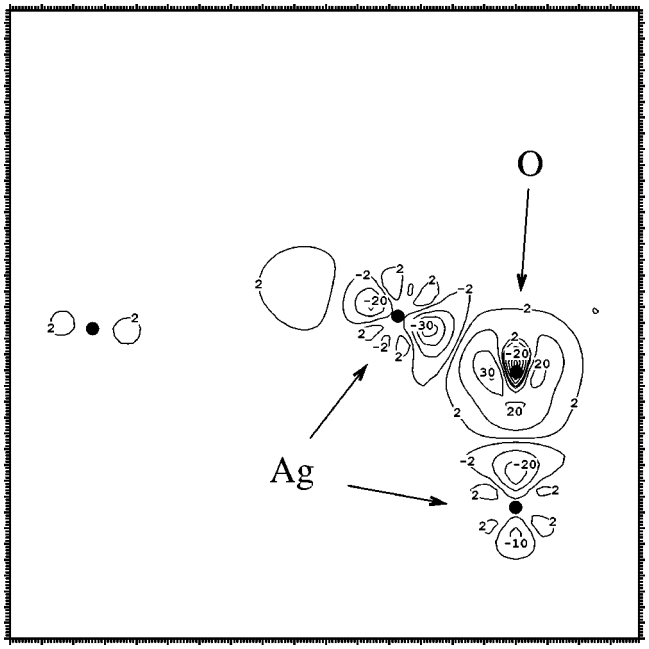

FIG. 3. The difference in electron density, $n(\mathbf{r})^{\Delta}$, (see the definition in Ref. 32) for oxygen in the subsurface tetra-I site for coverage 0.25 ML. The contour plane is in the [211] direction and is perpendicular to the Ag(111) surface and intersects the Ag atoms. The unit is 10^{-3} Bohr^{-3}. The positions of the O and Ag atoms are indicated by the arrows.

The O-Ag bondlengths are generally longer for the case of the octa site compared to the tetra sites, which is in-line with the understanding that adsorbates in higher coordinated sites have longer bondlengths compared to lower coordination sites.[40,42] Most of the O-Ag bondlengths involving subsurface oxygen are longer than the typical bondlength between on-surface oxygen and Ag (2.17 Å), i.e., roughly 8.8, 2.3, 2.8 % longer for the octa, tetra-I, and tetra-II sites, respectively.

The change in the work function induced by subsurface oxygen is modest, i.e., less than 0.56 eV for all of the adsorption sites throughout the range of coverages considered, which is in strong contrast to the case of on-surface oxygen adsorption, where it is as large as 4 eV at 1.00 ML.[32] This is due to the location of O under the surface Ag layer, which screens well the partially negatively charged oxygen atoms, and in addition there is, to a large degree, a cancellation of dipole moments involving oxygen and the top two Ag layers as indicated by the difference in electron density in Fig. 3. The electron density of the exposed (surface) silver atoms and the silver atoms bonded to O in the second layer, is depleted, while there is a large accumulation on the O atom. The result is very similar for the octa site.

Similarly to on-surface oxygen adsorption,[32] the interaction between subsurface oxygen and silver is mainly via hybridization of the O-$2p$ and Ag-$4d$-$5sp$ states, where antibonding states are largely occupied, indicating an ionic

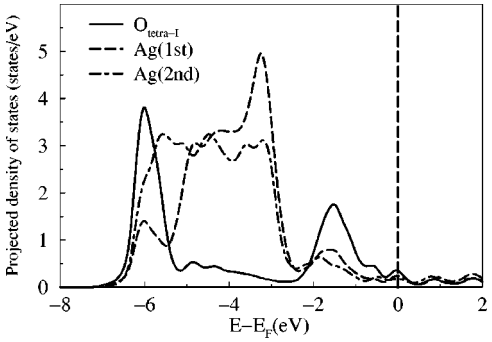

FIG. 4. Total PDOS for oxygen in the subsurface tetra-I site for coverage 0.25 ML. The Ag PDOS of the first and second metal layer atoms that are bonded to oxygen are indicated by dashed and dot-dashed lines, respectively, and the O PDOS is indicated by a solid line. The vertical dashed line marks the Fermi energy.

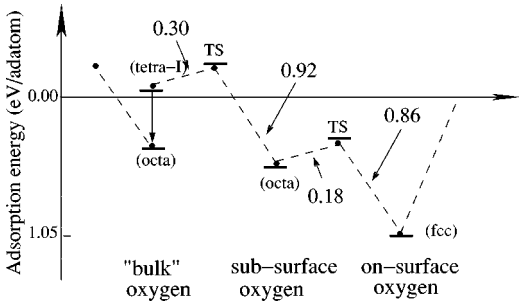

FIG. 5. Adsorption energy of oxygen at a coverage of 0.11 ML for penetration into the subsurface octa site from the on-surface fcc-hollow site through the first Ag layer, and from the octa site to the ''bulk'' tetrahedral site, through the second Ag layer (from right to left). From the tetra-I site, O will move to the more favorable bulk octa site under the second Ag layer. The short lines indicate the adsorption energy with respect to half of the binding energy of the oxygen molecule (experimental value). ''TS'' represents the transition states, and the numbers on the arrows indicate the energy barriers.

nature and explaining the relatively weak binding energy compared to the metals to the left of Ag in the periodic table. This can be seen from the total projected density of states of the O atom and of the Ag atoms in the first and second layers that are bonded to O, as shown in Fig. 4 for oxygen in the tetra-I site at coverage 0.25 ML. The band width of the Ag-4*d* states are notably narrower for the surface Ag atoms due to the lower coordination. As for on-surface oxygen adsorption, no other peaks occur between the O-2*s* state and the lower edge of the Ag-4*d* band; we point this out because such a feature has been found in some experimental studies, the origin of which is under debate (see, e.g., Ref. 2). Clearly, purely subsurface oxygen is not responsible for these features, nor is purely on-surface oxygen or surface-substitutional oxygen.[32] This will be discussed in more detail in Sec. V B. Compared to on-surface oxygen, the O-2*s* PDOS for subsurface oxygen is at a *lower* energy, which, from the initial state theory of core-level shifts, indicates that subsurface oxygen is less negatively charged.

C. Energy barriers for O penetration into the substrate

To investigate subsurface oxygen in more detail with regard to the energetics of its formation, we study the penetration of O through the surface Ag layer from the on-surface (fcc) site to the subsurface octahedral site at low coverage (0.11 ML). The transition state corresponds to the oxygen atom in the plane of the surface Ag(111) layer. We fully relax the first three Ag layers, but to stay at the transition state, we restrain O to be in the plane of the first Ag(111) layer (if we did not do this, the O atom would move to one of the two minima either side). The vertical distance of this top layer, however, is relaxed. We also considered the diffusion barriers for oxygen under the first Ag layer to move deeper into the bulk, i.e., to diffuse through the second Ag layer by analogous calculations. In this case, the pathway is from the octa site under the first Ag layer to the tetra-I site under the second Ag layer. Oxygen will then move to the energetically more favorable octa site under the second Ag layer. We note that due to the use of a (3×3) surface cell, which will restrict complete lateral relaxations at the transition state, the barriers could be slightly lower. The present values may be taken as an upper limit. From Fig. 5 it can be seen that the energy barrier for fcc oxygen to enter the subsurface region is 0.86 eV. For the reverse process, i.e., to diffuse to the surface from the octa site, the barrier is only 0.18 eV. Assuming that the prefactor for the two diffusion directions is the same, and using a simple Arrhenius equation, the ratio of the diffusion coefficients for movement from the surface to the subsurface, compared to from the subsurface to the surface is 5.1×10^{-8} at 470 K and 1.6×10^{-4} at 900 K. These kinetic considerations indicate that chemisorbed oxygen will stay on the surface at low coverage and at temperatures of around 470 K. Even at the higher temperature of 900 K, the difference is still significant.

The obtained energy barrier to move deeper into the bulk from under the first Ag layer to under the second Ag layer is 0.92 eV. This value is slightly larger compared to the case of oxygen diffusing through the first metal layer; this is due to the presence of the surface in that it costs less energy for the surface Ag atoms to relax compared to the Ag atoms in the second layer, which are more constricted due to other Ag atoms both above and below. Although configurational entropy for O in the bulk could drive oxygen to diffuse deeper into bulk region, the above results clearly show that there is a large potential gradient indicating that the oxygen, in the lower coverage regime, will be concentrated near surface.

As noted in the introduction, a chemisorbed oxygen species at coverage 0.05 ± 0.03 ML was observed, by scanning tunneling microscopy (STM).[31] The associated feature exhibited a depression with a diameter of 9 ± 1 Å which, according to the STM stimulation, suggested that the oxygen atom is located in the octa site under the first silver layer. On-surface adsorption was excluded since the diameter of the depression in the stimulations was significantly less, i.e., just 4 ± 1 Å. The tetra-I site was excluded on the basis that it offered less space and was expected to be energetically unfavorable. The alternative tetra-II site was not mentioned. No calculations, however, of energies were performed in this study. As our results show, at coverage 0.11 ML, the binding

energy of O on the surface is energetically significantly more favorable than sub-surface oxygen which does not support this assignment. The effective O-O repulsion is not very strong in the coverage range 0.06–0.11, i.e., the adsorption energy is only 0.05 eV smaller for the latter coverage (see Fig. 14). Thus we believe that for the lower coverage of 0.05 ML, the energetic preference for on-surface adsorption will not change.

IV. EFFECT OF SUBSURFACE OXYGEN

In the preceding section it was shown how on-surface oxygen was energetically favorable for coverages less than ≈ 0.50 ML compared to pure sub-surface adsorption, but for higher coverages, subsurface adsorption was preferred. It was also seen how the presence of subsurface oxygen changes the nature of the surface Ag atoms, namely, by causing a depletion of the electron density. In order to investigate the effect that subsurface oxygen has on the reactivity of the surface, as a first step we study the adsorption of additional oxygen on the surface with subsurface O present. This study is interesting in the sense that if on-surface oxygen is taken to represent an arbitrary electronegative adparticle, its behavior may reflect a general tendency. Investigating the interaction between on-surface and subsurface oxygen is also essential in relation with understanding the initial formation of surface oxides. We first consider many different atomic arrangements involving structures with an O atom on the surface and one under the surface Ag layer in order to identify energetically favorable geometries.

A. Energetics

We consider the case of one on-surface oxygen atom in the fcc site O_{fcc} of the (2×2) cell plus one subsurface oxygen atom, i.e., a total coverage of 0.50 ML. With this arrangement, there are three high-symmetry subsurface sites, namely, octa, tetra I, and tetra II, as described above, but due to the presence of O_{fcc}, there are now *two* different kinds of each of these sites, which can be differentiated by their relative distance to O_{fcc}. We therefore assign the label ''1nn'' (first nearest neighbor) to indicate the three subsurface sites closest to O_{fcc} and ''2nn'' to indicate those that are the second nearest-neighbor subsurface sites. These six possible subsurface sites are shown in Fig. 6. We tested all of these possibilities, where the positions of the oxygen atoms and top three silver metal layers were fully relaxed. Similar geometries exist when on-surface oxygen is located in the hcp-hollow site; in the light of what is learnt from the results for O in the fcc site, however, we viewed it necessary to only consider two structures for this case.

We first discuss results of subsurface adsorption with on-surface O in fcc sites. The calculated (average) adsorption energies are given in Table II, along with the removal energies [cf. Eqs. (2) and (3)], and the O-Ag bondlengths and metal interlayer expansions, as well as the work function change.

It can be seen that the values depend strongly on the location of subsurface oxygen: The average adsorption energies vary from 2.77 to 3.27 eV. Furthermore, the 1nn set of structures are energetically unfavorable compared to the 2nn set. This is due to the close proximity of the former to O_{fcc} which causes a considerable O-O repulsion. For example, the adsorption energy of the *most favorable* structure of the 1nn set is 2.92 eV, while the *least favorable* structure of the 2nn set is 2.99 eV. The energetically most favorable structure of all is that where subsurface oxygen is located in the tetra-I site of the 2nn set. This structure is denoted as $(O_{fcc}/O_{tetra\text{-}I})_{\theta=0.50}$ and can be seen more clearly in Fig. 10(b).

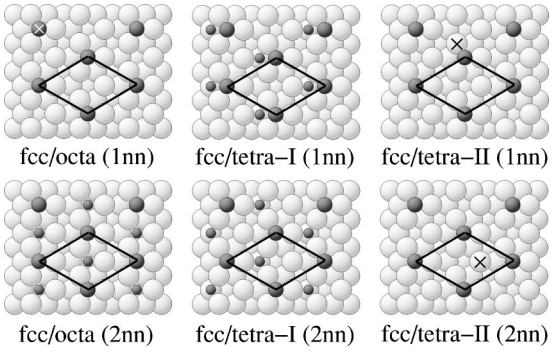

FIG. 6. Schematic geometry of the (2×2) surface unit cells with on-surface oxygen in the fcc site O_{fcc} (larger dark circles) for a coverage of 0.25 ML. The various subsurface sites are depicted as the small dark circles and the resulting on-surface+subsurface geometries defined by the label [e.g. fcc/octa (1nn)]. There are two different types of subsurface sites; ones that are closest to O_{fcc}, denoted 1nn and ones that are further away, denoted 2nn. Note, as indicated by the 'x' on the atoms, the 1nn-O_{octa} site is located directly below O_{fcc} and the tetra-II site is located directly below surface Ag atoms.

To investigate the effect of subsurface oxygen on the bond strength of O_{fcc}, we consider the removal energy cf. Eq. (2). We calculated this quantity for O in all of the various subsurface sites. For subsurface O in the octa, tetra-I, and tetra-II sites of the 1nn set, the respective removal energies are 2.98, 2.94 and 3.36 eV. For the same sites but in the 2nn set, the values are 3.10, 3.93, and 3.64 eV, respectively. These values can be compared to the adsorption energy of O_{fcc} (at 0.25 ML) without the presence of subsurface oxygen which is 3.52 eV.[32] Thus, depending on the location of subsurface oxygen, it can be either *destabilize or stabilize* significantly the interaction between on-surface oxygen and the metal substrate. The energetically most stable structure $(O_{fcc}/O_{tetra\text{-}I})_{\theta=0.50}$, *stabilizes* on-surface O by 0.41 eV (compare 3.93 to 3.52 eV). The effect of the presence of on-surface O on the binding of subsurface O [cf. Eq. (3)] is like that found for the effect of subsurface O on the binding of on-surface O. This can be seen from the inspection of the values of $E_{sub}^{removal}$ in Table. II, together with the values of E_{ad} in Table I for structures involving purely subsurface oxygen.

For on-surface oxygen in the hcp-hollow site, we considered the octa and the tetra-I sites of the 2nn set for subsurface O. The former, denoted as $(O_{hcp}/O_{octa})_{\theta=0.50}$, is geometrically very similar to the energetically favorable structure $(O_{fcc}/O_{tetra\text{-}I})_{\theta=0.50}$, namely, both involve a linear O-Ag-O

TABLE II. Calculated atomic geometries, energetics, and work function change for oxygen adsorption in structures involving both on-surface fcc-hollow sites and subsurface sites at a total coverage of 0.50 ML. R_1^{on} is the bondlength between on-surface oxygen and silver atoms in the first metal layer, while R_1^{sub} is the bondlengths between subsurface oxygen and silver atoms in the first metal layers. d_{12} is the first metal interlayer distance given with respect to the center of gravity of each layer. The bulk interlayer distance is 2.43 Å. E_{ad} is the average adsorption energy with respect to atomic oxygen, while $E_{on}^{removal}$ and $E_{sub}^{removal}$ are the removal energies for on-surface and subsurface oxygen atoms, as defined in Eqs. (2) and (3). $\Delta\Phi$ is the change in work function with respect to the clean surface (calculated to be 4.45 eV). The unit of length is Å and of energy is eV.

	R_1^{on}	R_1^{sub}	d_{12}	E_{ad}	$E_{on}^{removal}$	$E_{sub}^{removal}$	$\Delta\Phi$
1nn							
fcc/octa	2.17	2.46	2.73	2.92	2.98	2.33	1.81
fcc/tetra-I	2.19	2.18	2.81	2.77	2.94	2.03	1.52
fcc/tetra-II	2.18	2.26	2.80	2.90	3.36	2.29	1.10
2nn							
fcc/octa	2.19	2.26	2.72	2.99	3.10	2.44	1.40
fcc/tetra-I	2.10	2.09	2.89	3.27	3.93	3.02	1.15
fcc/tetra-II	2.21	2.17	2.84	3.05	3.64	2.58	0.84
hcp/octa	2.15	2.11	2.78	3.33	3.80	3.25	1.02
hcp/tetra-I	2.16	2.18	2.86	2.77	2.94	2.14	1.59

bonding arrangement. And as can be seen from the results presented in Table II, it is also a low-energy structure; in fact, it is the lowest of all. That it is slightly more favorable (by 0.06 eV) may be understood due to the fact that the pure subsurface O_{octa} structure at 0.25 ML is energetically more favorable than the $O_{tetra\text{-}I}$ site (by 0.24 eV) as shown in Table I, while the difference between pure on-surface O_{fcc} and O_{hcp} is less (0.11 eV).

Comparing the average adsorption energies of the structures described above for coverage 0.50 ML to the structures at same coverage, but where oxygen occupies exclusively either on-surface ($E_{ad}=2.92$ eV for fcc oxygen) or subsurface sites ($E_{ad}=2.94$ eV for O_{octa}), it is found that the mixed structures $(O_{fcc}/O_{tetra\text{-}I})_{\theta=0.50}$ (3.27 eV) and $(O_{hcp}/O_{octa})_{\theta=0.50}$ (3.33 eV) are significantly energetically *more favorable*. The average adsorption energies of these mixed structures are, however, not greater than that of on-surface adsorption at the lower coverage of 0.25 ML. Other geometries are also possible for coverage 0.50 ML, for example, pure on-surface O involving hcp and fcc sites $(O_{fcc}+O_{hcp})_{\theta=0.50}$ and pure subsurface O in different sites $(O_{octa}+O_{tetra\text{-}II})_{\theta=0.50}$ and $(O_{tetra\text{-}I}+O_{tetra\text{-}II})_{\theta=0.50}$ where the two subsurface oxygen atoms are separated as far as possible from each other. All these geometries were tested and found to be energetically unfavorable, as shown by their respective average adsorption energies, namely, 2.41, 2.94, and 2.95 eV (cf. Table III). Altogether, our calculations indicate that oxygen will enter the subsurface region for coverages greater than 0.25 ML. We note that this coverage could be less, but to determine this would require the use of larger supercells; the value of $\theta=0.25$ ML may therefore be regarded as an upper limit. Clearly, this is in contrast to O adsorption on Ru(0001) where O adsorption in subsurface sites only becomes energetically preferred after the completion of a full monolayer.[16,17]

Viewing oxygen as a typical electronegative atom, its function at the subsurface site may be replaced by other electronegative species, such as chlorine, which is actually used as a promoter in some reactions that silver catalyses.[1] It may be expected then that chlorine will also stabilize on-surface electronegative species. Also, the found enhanced stability of on-surface oxygen due to subsurface O may also reflect the behavior of other similar species at the surface. This could explain the reported stabilization of CO on Ag(100) which was attributed to subsurface oxygen.[43]

B. Atomic structure and electronic properties

In the following we describe the main structural and electronic properties of the energetically most favorable on-surface+subsurface structures. Full details concerning the O-Ag bondlengths and metal interlayer spacing are given in Table II. The most notable feature of the low-energy structures is a characteristic linear O_{on}-Ag-O_{sub} bonding arrangement of the uppermost atoms. In-line with their energetic preference, they also have shorter O-Ag bondlengths; for example, for $(O_{fcc}/O_{tetra\text{-}I})_{\theta=0.50}$ the O_{fcc}-Ag bondlength, R_1^{on}, and the bondlength of subsurface O to the first Ag layer, R_1^{sub}, are 2.10 and 2.09 Å, respectively, and for $(O_{hcp}/O_{octa})_{\theta=0.50}$, the analogous values are 2.15 and 2.11 Å, respectively. These can be seen from the inspection of Table II to be shorter than the less favorable on-surface +subsurface geometries. They are also shorter compared to the corresponding bondlengths of the pure on-surface and pure subsurface structures, e.g., 2.17 Å for on-surface fcc oxygen, 2.12 for $O_{tetra\text{-}I}$, and 2.24 Å for O_{octa} at coverage 0.25 ML. Compared to the values of R_1^{sub} (bondlengths of subsurface O to the top Ag layer), for the two most favorable structures, the bondlengths of subsurface oxygen to the *second* Ag layer (not shown here) are pronouncedly longer,

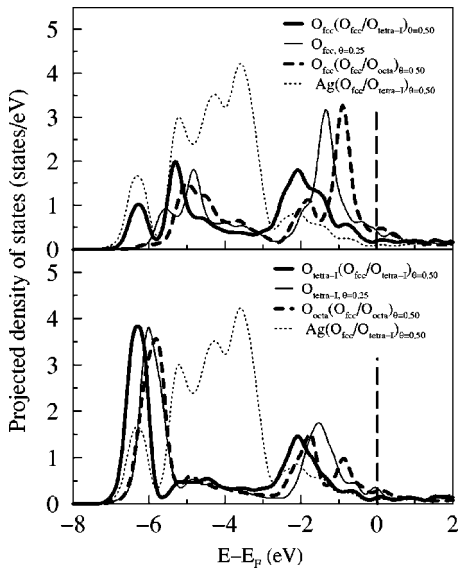

FIG. 7. Total projected density of states (PDOS) for the favorable $(O_{fcc}/O_{tetra\text{-}I})_{\theta=0.50}$ and unfavorable $(O_{fcc}/O_{octa})_{\theta=0.50}$ structures. PDOS for O_{fcc} (upper figure) and $O_{tetra\text{-}I}$ (lower figure) are shown by thick solid lines, and the silver atoms shared by the two oxygen atoms are shown as dotted lines. For comparison, O_{fcc} without the presence of subsurface oxygen (thin solid line) and with subsurface oxygen in the octa site (thick dashed line) are shown in the upper figure. Also for comparison (lower figure) are the PDOS for $O_{tetra\text{-}I}$ without on-surface oxygen (shown as thin solid line) as well as subsurface O in the octa site of the unfavorable structure (thick dashed line). The energy zero is the Fermi energy.

which indicates a stronger bonding of subsurface O to the *surface* Ag layer, which is also bonded to a surface O atom.

In Table II, the work function changes with respect to the clean Ag(111) surface due to O adsorption for the on-surface +subsurface structures described above are listed. The values vary from 0.84 to 1.81 eV, and for the energetically most favorable structures the values are $(O_{fcc}/O_{tetra\text{-}I})_{\theta=0.50}$ 1.15 eV and $(O_{hcp}/O_{octa})_{\theta=0.50}$, 1.02 eV, respectively. For comparison, the change in work function for on-surface oxygen at coverage 0.25 ML are 1.23 eV (fcc) and 1.31 eV (hcp),[32] and the values of the work function for the on-surface fcc and hcp sites at the same coverage of 0.50 ML are more than twice as large as the structures involving both on-surface and subsurface oxygen.[32] Subsurface O competes with on-surface oxygen for the bonding charge of the surface Ag atoms; as a consequence, the on-surface O species are slightly *less negatively charged* compared to when there is no subsurface O. This can be seen by comparing Fig. 8 (below) with that of Fig. 4 in Ref. 32, and is also indicated by the lower-energy position of the O-2*s* levels for the favorable on-surface+subsurface structure as discussed below.

In Fig. 7 we show the projected density of states for O_{fcc} and $O_{tetra\text{-}I}$ atoms of the energetically favorable $(O_{fcc}/O_{tetra\text{-}I})_{\theta=0.50}$ structure. They are labeled "$O_{fcc}(O_{fcc}/O_{tetra\text{-}I})_{\theta=0.50}$" and "$O_{tetra\text{-}I}(O_{fcc}/O_{tetra\text{-}I})_{\theta=0.50}$," respectively, and are denoted by thick continuous lines in the upper and lower parts of the figure. We also show the PDOS for the first layer silver atoms which are bonded to these two O atoms (dotted lines in Fig. 7). For comparison we show the PDOS for the O_{fcc} and O_{octa} atoms of the energetically *unfavorable* $(O_{fcc}/O_{octa})_{\theta=0.50}$ structure (thick dashed curves in the upper and lower parts of the figure, respectively), as well as the PDOS for the structures containing purely O_{fcc} (i.e., without $O_{tetra\text{-}I}$) and purely $O_{tetra\text{-}I}$ (i.e., without O_{fcc}) atoms.

Considering first the results of $(O_{fcc}/O_{tetra\text{-}I})_{\theta=0.50}$, it can be seen that the PDOS for O_{fcc} of this structure is shifted to a lower energy compared to the pure on-surface O_{fcc} species (compare the thick and thin continuous lines, respectively, in the upper plot). The antibonding states of O_{fcc} of the $(O_{fcc}/O_{tetra\text{-}I})_{\theta=0.50}$ structure are around 0.74 eV lower compared to the case of pure O_{fcc}. A similar shift occurs for the O-2*s* state. For $O_{tetra\text{-}I}$ of the $(O_{fcc}/O_{tetra\text{-}I})_{\theta=0.50}$ structure, as compared to $O_{tetra\text{-}I}$ of the pure subsurface $O_{tetra\text{-}I}$ at 0.25 ML, it exhibits a similar behavior, but the magnitude of the shift is less, i.e., around 0.56 eV for the valence PDOS and 0.45 eV for the 2*s* state. Due to the mentioned shifts to lower energies, the DOS at the Fermi energy decreases for the $(O_{fcc}/O_{tetra\text{-}I})_{\theta=0.50}$ system compared to that not containing subsurface oxygen. This is also the case for the *total* DOS. The density of states for the other energetically favorable structure $(O_{hcp}/O_{octa})_{\theta=0.50}$ (not shown) are very similar to that of $(O_{fcc}/O_{tetra\text{-}I})_{\theta=0.50}$ which is in-line with their similar energetics.

We now consider an *energetically unfavorable* configuration for comparison, namely $(O_{fcc}/O_{octa})_{\theta=0.50}$ (where O_{octa} is in the 2nn set of O_{fcc}, see Fig. 6 and Table II). A different behavior to that described above is found: Here the PDOS for on-surface oxygen (O_{fcc}) shifts towards *higher* energies with the presence of subsurface O, as does the O-2*s* state (compare the thick dashed and thin continuous lines in the upper plot of Fig. 7). Furthermore, we find that all the energetically unfavorable structures exhibit a higher total DOS at the Fermi level compared to the energetically favorable ones.

To gain further insight into the bonding mechanism, we calculate the difference in electron density distribution for $(O_{fcc}/O_{tetra\text{-}I})_{\theta=0.50}$, as shown in Fig. 8. A depletion of Ag-4$d_{xz,yz}$ states of the surface silver atoms bonded to the O_{fcc} and $O_{tetra\text{-}I}$ oxygen atoms occurs, while there is an increase in electron density on the O atoms. The coupling between $O_{tetra\text{-}I}$ and the silver atom directly below in the second metal layer is comparably weak, as indicated by the modest perturbation of electron density, and as also suggested by the longer bondlength described above. It is the O_{fcc}-Ag-$O_{tetra\text{-}I}$ linear coordination that allows a strong hybridization of the Ag-4$d_{xz,yz}$ orbital with the O_{fcc} and $O_{tetra\text{-}I}$ species, and also screens well the electrostatic interaction between them. This is also the case for the $(O_{hcp}/O_{octa})_{\theta=0.50}$ system (not shown) which contains the same linear coordination (i.e., O_{hcp}-Ag-O_{octa}) and weaker coupling to the substrate underneath.

The energetic preference for the fcc/tetra-I and hcp/octa (i.e., a linear O-metal-O) arrangement is found also at higher coverage. In particular, we also considered oxygen coverages of 2.00 ML. These structures involve a full monolayer on the surface and full monolayer under the first Ag layer, where there are a total of six possible configurations. We tested all of these and as mentioned above, the energetically favorable

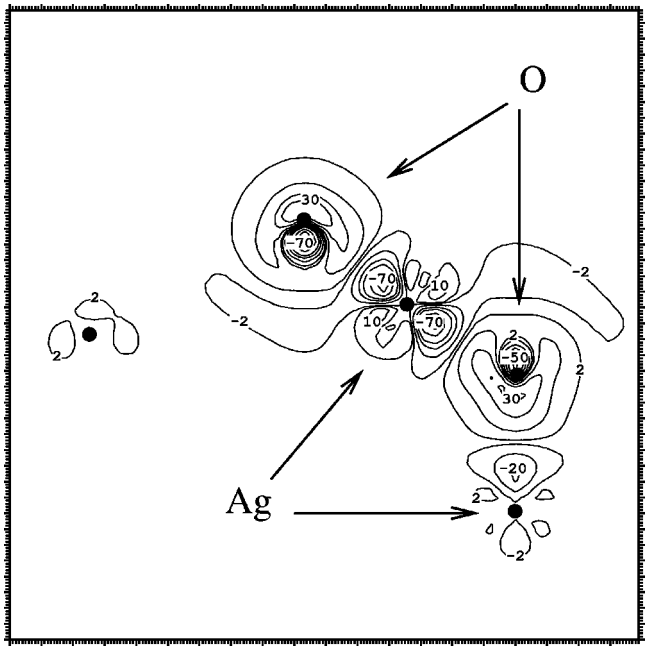

FIG. 8. The difference in electron density, $n(\mathbf{r})^{\Delta}$ (see the definition in Ref. 32) for $(O_{fcc}/O_{tetra\text{-}I})_{\theta=0.50}$. The contour plane is in the [211] direction and is perpendicular to the Ag(111) surface and intersects the Ag atoms. The unit is 10^{-3} Bohr^{-3}. The positions of the O and Ag atoms are indicated by the arrows.

structure is again that involving on-surface O in the hcp site and subsurface O in the octa site $(O_{hcp}/O_{octa})_{\theta=2.00}$ (by 0.07 eV), and the next most favorable structure is that for on-surface O in the fcc sites and sub-surface O atoms in the tetra-I sites $(O_{fcc}/O_{tetra\text{-}I})_{\theta=2.00}$. The average adsorption energies of these structures, are however, unstable with respect to gas phase O_2. Such linear O-metal-O geometries have also been found to be the most energetically favorable of those considered for other transition metals, e.g., Ru[18] and Rh.[19] As will be seen below, this is actually the primary building block involved for the energetically favorable structures involving higher oxygen concentrations as well as in silver(I) oxide Ag_2O. In addition, oxygen adsorption on Ag(110) with $(n\times1)$ reconstructions[44] involve a similar O-Ag-O configuration.

C. The (4×4)-O/Ag(111) phase

The proposed atomic geometry for the (4×4)-O/Ag(111) phase[30,31] bears a very close resemblance to the identified low-energy $(O_{fcc}/O_{tetra\text{-}I})_{\theta=0.50}$ structure. The difference being that the surface Ag atoms of the former structure are *not* commensurate with the underlying (1×1) surface unit cell, i.e., the upper O-Ag-O ''trilayer'' is laterally expanded to equal that of the (111) surface of bulk Ag_2O. In addition, to avoid Ag atoms sitting in top sites directly on top of the underlying Ag atoms, these Ag atoms are missing, i.e., one per (4×4) cell. This results in a stoichiometry of the trilayer of $Ag_{1.83}O$ with a corresponding oxygen coverage of 0.375 ML (see Fig. 9). We calculated the average O adsorption energy of this structure (including full atomic optimization)

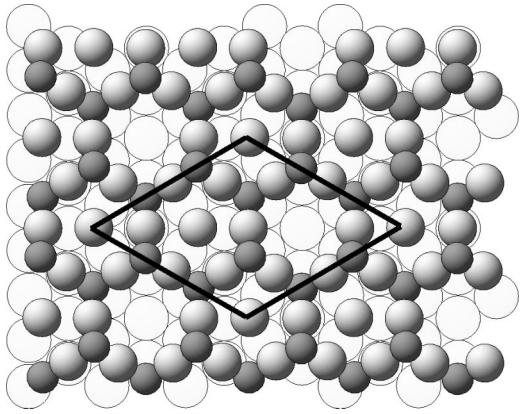

FIG. 9. Sketch of the atomic structure proposed in the STM study of Ref. 30 for the (4×4) phase. The surface unit cell is indicated. The oxygen atoms are represented by small dark circles, the uppermost Ag atoms by gray circles, and the intact plane of Ag(111) atoms lying below the ''O-Ag-O'' trilayer are represented as the open circles.

and find that it has a low energy (see Fig. 14). In obtaining this value, we have used the chemical potential of Ag in bulk to take into account the energy of the Ag atoms in the mixed trilayer. We also considered a ''stoichiometric structure,'' i.e., corresponding to Ag_2O within the trilayer in which the Ag atoms sitting on top of underlying substrate atoms are present and found, in agreement with other recent calculations of these two geometries,[45] that it is less favorable by 0.7 eV per cell.

V. FORMATION OF A SURFACE OXIDE

A. Accumulation of oxygen in the subsurface region

In order to gain insight into the stability of structures with higher concentrations of oxygen, we performed calculations for many different geometries. Since there are no experimental results to provide guidance, and no additional ordered phases observed, we use (2×2) surface cells and systematically investigate the many possible atomic configurations at the given coverages. Such a study would be unfeasible with the larger (4×4) cells, and given the very similar local atomic geometry mentioned above of the proposed (4×4) structure and our identified low-energy structure at 0.5 ML (and similar electronic structure), we view this as an appropriate strategy.

We first investigate various geometries involving 0.75 ML. Considering the addition of another O atom to the energetically favorable systems with total O coverage 0.50 ML, our results show that oxygen will occupy subsurface sites rather than on-surface sites to avoid the strong dipole-dipole repulsion. As seen in Table III, for the energetically favorable configuration described above for 0.50 ML of oxygen $(O_{hcp}/O_{octa})_{\theta=0.50}$, the addition of an O atom to the on-surface hcp site yields an average binding energy of 2.97 eV, but it is 3.25 eV if the additional O atom occupies the subsurface octa site below the first Ag layer $(O_{hcp}/O_{octa})_{\theta=0.75}$. A similar result is found for the other energetically favorable structure at 0.50 ML $(O_{fcc}/O_{tetra\text{-}I})_{\theta=0.50}$, in that it is ener-

TABLE III. Average adsorption energy (per oxygen atom) E_{ad} and work function change $\Delta\Phi$, for oxygen in various sites and for various coverages. θ_{sub}, θ_{on}, and θ_{total} represent the oxygen coverage in the subsurface and on-surface regions, and the total coverage, respectively. The energy unit is eV.

	θ_{on}	θ_{sub}	E_{ad}	$\Delta\Phi$
$\theta_{total}=0.25$				
fcc	0.25	-	3.52	1.23
octa	-	0.25	2.85	0.09
$\theta_{total}=0.50$				
fcc	0.50		2.92	2.22
hcp	0.50		2.83	2.36
fcc+hcp	0.50		2.41	2.53
octa		0.50	2.94	0.09
octa+tetra II		0.50	2.94	0.02
tetra-I+tetra II		0.50	2.95	0.27
octa+tetra I		0.50	2.78	0.46
fcc/tetra I	0.25	0.25	3.27	1.15
hcp/octa	0.25	0.25	3.33	1.02
$\theta_{total}=0.75$				
hcp/octa	0.50	0.25	2.97	2.22
hcp/octa	0.25	0.50	3.25	1.42
hcp/octa+tetra II	0.25	0.50	3.26	0.85
fcc/tetra I	0.50	0.25	2.90	2.19
fcc/tetra I	0.25	0.50	3.06	1.47
fcc/tetra I+tetra II	0.25	0.50	3.29	0.98
$\theta_{total}\geqslant 1.00$				
hcp/octa	0.25	0.75	3.09	1.63
hcp/octa	0.25	1.00	2.89	1.58
fcc/tetra I+tetra II /tetra I	0.25	0.75	3.13	0.66
fcc/tetra I+tetra II /tetra I+tetra II	0.25	1.00	3.22	1.02
fcc/tetra I+tetra II . . . /tetra I+tetra II	0.25	2.00	3.21	1.17

getically favorable for the additional oxygen atom to occupy a subsurface site, namely, the tetra-I site $(O_{fcc}/O_{tetra\text{-}I})_{\theta=0.75}$ (3.06 eV), instead of an on-surface fcc-hollow site (2.90 eV). The reason that the average binding energy of $(O_{hcp}/O_{octa})_{\theta=0.75}$ with 0.50 ML octa oxygen is 0.19 eV more favorable than $(O_{fcc}/O_{tetra\text{-}I})_{\theta=0.75}$ with 0.50 ML tetra-I oxygen, is mainly due to the difference in energy of the pure subsurface O_{octa} and the pure subsurface $O_{tetra\text{-}I}$ structures at coverage 0.50, which as shown in Table I, is 2.57 eV for the latter and 2.94 eV for the former.

We also tested if it is energetically more favorable for the two subsurface O species to occupy different types of subsurface sites. For instance, as shown in Table III, $(O_{octa}+O_{tetra\text{-}II})_{\theta=0.50}$ and $(O_{tetra\text{-}I}+O_{tetra\text{-}II})_{\theta=0.50}$ have average adsorption energies of 2.94 and 2.95 eV, respectively, very close to O_{octa} at same coverage (2.94 eV). We find that the energetically most favorable structures at coverage 0.75 ML do involve subsurface O atoms in different sites, in addition to that where they both occupy the octa site, namely $(O_{hcp}/O_{octa}+O_{tetra\text{-}II})_{\theta=0.75}$, with average adsorption energy 3.26 eV $(O_{fcc}/O_{tetra\text{-}I}+O_{tetra\text{-}II})_{\theta=0.75}$ with average binding energy 3.29 eV, as well as $(O_{hcp}/O_{octa})_{\theta=0.75}$ (3.25 eV).

Interestingly, the slightly more favorable one $(O_{fcc}/O_{tetra\text{-}I}+O_{tetra\text{-}II})_{\theta=0.75}$ [depicted in Fig. 10(c)], is similar in structure to the bulk silver oxide Ag_2O, where both subsurface oxygen atoms are located at the center of a silver tetrahedron, and the silver atoms shared by the O atoms are in a linear chain. Within the accuracy of our calculations, however, these three structures are essentially degenerate.

B. Higher O concentrations and formation of an oxidelike film

We now consider the incorporation of higher concentrations of atomic oxygen. For a coverage of 0.75 ML the favored structures have 0.25 ML oxygen on the surface and 0.50 ML between the first and second Ag layers. We will now determine the energetic preference for adding one more O atom and then subsequently a second one, resulting in total coverages of 1.00 ML and 1.25 ML, respectively. In particular, we will investigate whether oxygen will prefer to occupy the subsurface region under the first metal layer along with the two oxygen atoms already there, or if the O atoms will reside deeper in the ''bulk'' region, i.e., under the second metal layer.

The results are shown in the lower part of Table III. For additional oxygen occupation under the first Ag layer, as an example, we show that for the hcp/octa system the result for subsurface coverages of 0.75 and 1.00 ML with O in the octa site. The average adsorption energies are 3.09 and 2.89 eV, respectively. However, if these additional oxygen atoms occupy instead sites under the *second* Ag layer, in particular, according to the identified preference for a linear O-Ag-O bonding arrangement, then the average adsorption energies are 3.13 and 3.22 eV, respectively, which are clearly energetically more favorable compared to additional oxygen occupation under the first Ag layer. The latter structure is shown in Fig. 10(d), where it can be seen, in comparison with 10(b) and 10(c), that with continuous O incorporation, the same structure can keep forming. Actually, the average binding energy of 3.22 eV at coverage 1.25 ML, has already converged to the value of the structure at the higher coverage of 2.25 ML (3.21 eV), as shown at the end of Table III. This value is also very close to the calculated heat of formation for *bulk* Ag_2O, which is 3.23 eV (also referred to the free O atom).[46]

In Fig. 11, the work function change of the identified energetically favorable structures involving on-surface and subsurface oxygen, as well as that for the (4×4) structure are shown, where they are compared to the values of pure on-surface adsorption. It can be seen that they are significantly lower than for on-surface adsorption and vary between 1.1 to 0.5 eV. Interestingly these values are close to that of $\sim$1.0 eV as reported experimentally for Ag(111) when subjected to high oxygen pressures and high temperature.[9] The value for the (4×4) structure is also in very good agreement with the value of 0.55 eV reported by Bare *et al.*[47]

The identified energetically favorable structures with high O concentrations e.g., 1.25 ML or 2.25 ML are like silver(I) oxide $Ag_2O(111)$ but under a compressive lateral strain of

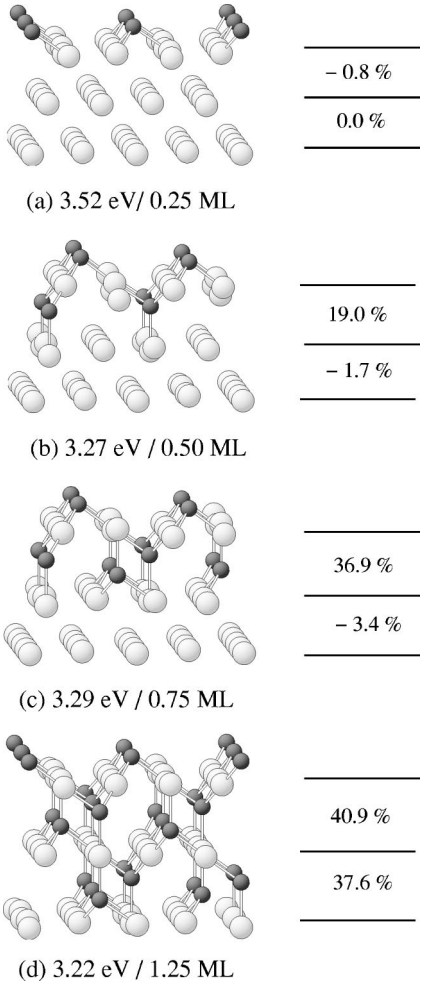

FIG. 10. Atomic geometry of energetically favorable structures for increasing oxygen concentrations: (a) on-surface fcc oxygen, (b) fcc oxygen plus subsurface oxygen in the tetra-I site, (c) as for (b) but with additional oxygen in the tetra-II site, (d) as for (c) but with additional oxygen under the second Ag layer in the tetra-I and tetra-II sites. The average adsorption energy with respect to the clean Ag(111) substrate and free oxygen atoms, as well as the corresponding coverage, are given at the bottom of each figure. The relative variation of the first and second interlayer spacings with respect to the bulk value is also given to the right of the figures. Large pale gray and small dark circles represent silver and oxygen atoms, respectively.

18%. The character of the oxide is already present for coverage 0.75 ML: In addition to the same local atomic coordination, the vibration of subsurface oxygen, $O_{\text{tetra-I}}$, in $(O_{\text{fcc}}/O_{\text{tetra-I}}+O_{\text{tetra-II}})_{\theta=0.75}$ is calculated to be 526 cm^{-1} which is very similar to the experimental value of 545 cm^{-1} for oxygen in bulk Ag_2O.[48] The calculated valence band for the oxidelike structure $(O_{\text{fcc}}/O_{\text{tetra-I}}+O_{\text{tetra-II}}/O_{\text{tetra-I}}+O_{\text{tetra-II}})_{\theta=1.25}$, shown in Fig. 12, also bears a close resemblance to that of bulk Ag_2O. The upper panel shows the result of the uppermost O_{fcc}-Ag-$O_{\text{tetra-I}}$ atoms, and the lower one shows the result for $O_{\text{tetra-II}}$ under the first metal layer and $O_{\text{tetra-I}}$ under the second metal layer, as well as the silver atom in the second layer to which they commonly bond. Compared to the clean surface, or lower coverage structures,

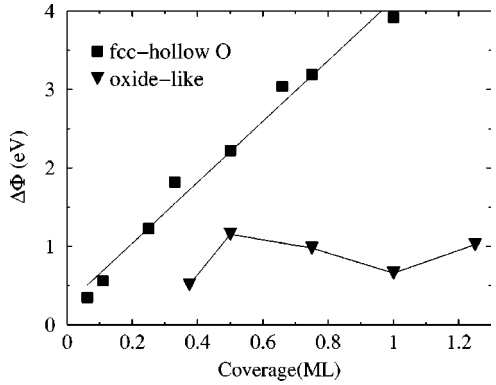

FIG. 11. Work function change for on-surface O adsorption in the fcc site (squares) (from Ref. 32) and of the (4×4) and the oxidelike structures with higher oxygen concentrations (triangles).

e.g. $(O_{\text{fcc}}/O_{\text{tetra-I}})_{\theta=0.50}$, as shown in Fig. 7, the silver $4d$ band has considerably narrowed due to the significant increase of the spacing between the metal layers and the weak hybridization with the O-$2p$ states. Also, two extended shoulders appear either side of it. These features are very similar to those of the the oxide surface under zero lateral strain, which will be reported in detail elsewhere.[46]

We calculated the removal energies of the on-surface oxygen of the favorable structures. The resulting energies are very similar to what we found for the favorable 0.50 ML on-surface+subsurface structures discussed above in Sec. IV, namely, they are all in the range of 3.90–4.01 eV. These bondstrengths are actually the strongest we have found for this system, and such species could be important for understanding how silver functions as an efficient oxidation catalyst.

1. Relative stability of the oxidelike structures

It has been seen above that the average O adsorption energies of the energetically favorable structures at $\theta=0.50$ and 0.75 ML are slightly greater than the heat of formation of the bulk oxide referred to atomic oxygen (compare 3.27 and 3.29 eV to 3.23 eV). For the higher concentration structures, the values are, however, extremely close (compare 3.22 and 3.21 to 3.23 eV). This is very interesting since the oxidelike structures, although similar in geometry to ideal $Ag_2O(111)$ surfaces, are laterally compressed by a large amount. To investigate why the energies are so close, e.g., whether the underlying Ag(111) surface plays a role, or if the distortion actually has little effect on the energetics, we study the relative stability of the oxidelike structures in comparison with true $Ag_2O(111)$ structures. In particular, we calculate free-standing $Ag_2O(111)$ layer structures under zero strain and under a compressive strain of 18%, which corresponds to the strain of our identified oxidelike structures due to being commensurate with the underlying Ag(111) surface.

For a thickness involving five metal layers, it is found that the true oxide is energetically *less* favorable by 0.05 eV per oxygen atom than the oxide film under the strain. For thicker films corresponding to seven metal layers, the energy difference between two structures decreases to just 0.005 eV per

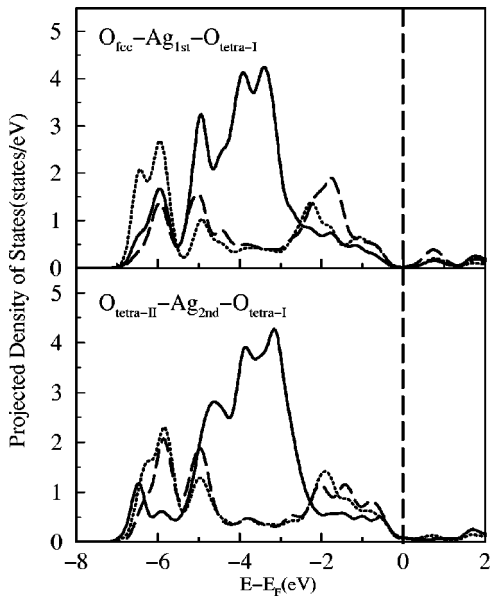

FIG. 12. Total projected density of states for the oxidelike structure $(O_{fcc}/O_{tetra_I}+O_{tetra\text{-}II}/O_{tetra_I}+O_{tetra\text{-}II})_{\theta=1.25}$. The upper figure shows the PDOS for O_{fcc} (dashed line), the uppermost Ag atoms bonded to both O atoms (solid line) and $O_{tetra\text{-}I}$ (dotted line) under the first layer. The lower figure shows the PDOS for $O_{tetra\text{-}II}$ (dashed line) under the first metal layer, the shared Ag atom (solid line) and $O_{tetra\text{-}I}$ (dotted line) under the second metal layer. The Fermi energy is indicated by the vertical dashed line.

oxygen atom, where the deformed oxide film is still preferred. Only for thicker structures involving nine metal layers does the true oxide film (zero strain) become energetically favorable (by 0.02 eV per oxygen atom). This could be taken to indicate that a transition to the natural oxide surface will only happen at or beyond a critical thickness corresponding to about nine metal layers. The transition may not occur immediately because the energy gain is still very small and it may take more layers in order for sufficient strain energy to build-up. Also, the interaction between the oxide structures and the metal substrate, which was not considered, may hinder the transition. That the structures with the smaller lateral dimensions are not notably less favorable than the true oxide structures can be understood in that there is a significant expansion normal to the surface, as shown in Fig. 10. For the O/Ru(0001) system,[18] from similar calculations, it was found that $RuO_2(110)$ layer structures become energetically more favorable compared to layers of the identified on-surface+subsurface structures with the same stoichiometry, after a thickness equivalent to only two or more metal layers. In this case the lateral deviation between the natural $RuO_2(110)$ oxide and the on-surface+subsurface structure was equal to 15% and 35% in the *y* and *x* directions, respectively, where the natural oxide is more expanded.

2. Adsorption of an ozonelike species

Another issue of debate in the literature is the origin of several electronic states observed lying in the energy region below the Ag-4*d* band and above the O-2*s* semi-core level. On one hand it has been proposed that hydroxl groups are responsible[2] and on the other hand an associatively adsorbed ozonelike species at a surface Ag vacancy has been proposed.[49] We investigated the latter species, the atomic geometry of which is shown in the insets of Figs. 13 and 14. We find, in agreement with Ref. 49, that the molecular ozonelike species is energetically preferred compared to three separate O atoms adsorbed at the vacancy edges. We considered two vacancy concentrations for the adsorption of the ozonelike species, namely, 0.11 and 0.33 ML, corresponding to O coverages of 0.33 and 1.0 ML, respectively. The atomic geometry is found to be similar to the ozone molecule in the gas phase, namely, when adsorbed on the surface the calculated bondlength between the O atoms is 1.41 Å and the angle is 118 deg, while for the free molecule the respective values are 1.27 Å and 117 deg. The longer bondlength between the O atoms when adsorbed on the surface indicates that the inter O-O bonding is weakened. The adsorption energy is very similar in each case, indicating that they interact little with each other. Compared to the oxidelike structures they are energetically unfavorable. However, if vacancies were provided ''for free'' (i.e. not taking into account the vacancy formation energy), then such a species is energetically favorable for $\theta=1.0$ ML (see Fig. 14). We expect, however, that the concentrations of vacancies will be rather low and this species will not be present in large concentrations.

With regard to the electronic structure, we find that there are indeed a number of electronic states in the energy regime below the bottom of the Ag-4*d* band as can be seen from Fig. 13, which shows the projected density of states on the O atoms. In particular, features are seen at energies of $\sim$2.0, 3.5, 6.0, 7.0, 8.5, 14.4, 19.5, 24.8 eV below E_F. Reported experimental features observed on polycrystalline silver are at 3.5, 9.2, and 11.2 eV below E_F, which were thought to be due to hydroxls,[2] and features observed for the O/Ag(110) system are at 3.3, 7.0, 9.5, 12.7, 17.3 eV, which were attribued to the associatively adsorbed ozonelike species.[49] It can be appreciated that there is some overlap of these various energies, but it is not possible to draw any solid conclusions on the basis of such comparisons.

In order to visually summarize the main energetics of our results, we show in Fig. 14 the average adsorption of oxygen at Ag(111) versus coverage. This also includes our earlier results for pure on-surface and surface-substitutional adsorption[32] as well as for investigations into bulk substitutional adsorption. There is one point in this figure not discussed in the present or previous (Ref. 32) paper so far and that is for the adsorption of an oxygen atom on the surface in the fcc site near a preexisting vacancy with coverage 0.25 ML. The adsorption energy is seen to be less favorable than on the ideal (111) terrace, but if such vacancies were provided for free (i.e., without paying the vacancy formation energy cost), it can be seen that their binding to the surface is considerably stronger than on the ideal (111) terrace, compare 3.83 eV to 3.52 eV. We expect a similarly stronger binding of O at other undercoordinated Ag atoms such as at the edge of steps or kinks, as has been found for other O/transition-metal systems. Considering Fig. 14, at a glance, these results predict that at low coverage, O prefers to adsorb

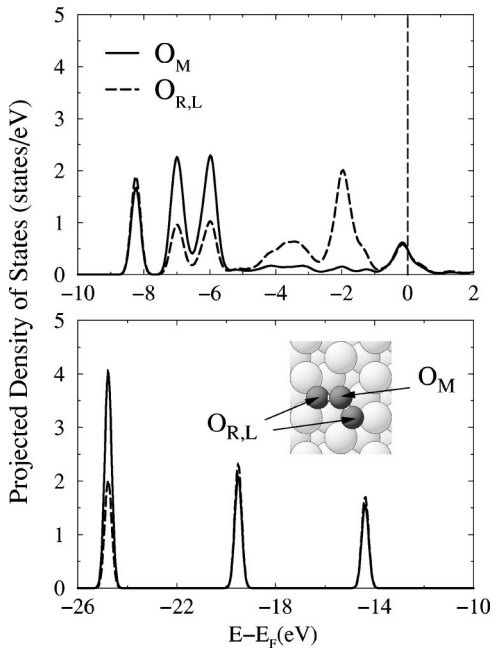

FIG. 13. Total projected oxygen density of states for the ozonelike species adsorbed at an Ag surface vacancy. The upper panel shows the valence-band energy region and the bottom panel, the lower-energy region. "O_M" indicates the center O atom of the ozonelike species and the "$O_{L/R}$" indicates the left and right O atoms of the ozonelike species that are bonded to two surface Ag atoms.

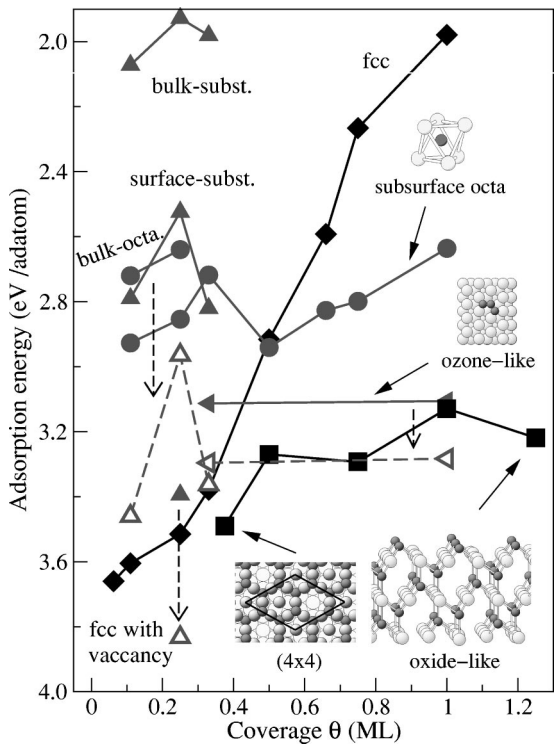

FIG. 14. Average adsorption energy (with respect to atomic O) versus coverage for the different structures considered: pure on-surface oxygen in fcc-hollow sites (diamonds), surface- and bulk-substitutional adsorption (triangles), pure subsurface oxygen in octahedral sites under the first (subsurface octa.) and second (bulk octa.) Ag layers (circles), an ozonelike molecule adsorbed at a surface Ag vacancy (left-pointing triangles), and surface oxidelike structures (squares), as illustrated in Fig. 10. The vertical downward pointing arrows directed at dashed lines with open symbols, indicate the corresponding *binding energies* of the structures involving surface Ag vacancies, i.e., the vacancy formation energy E_f^{vac} (see Ref. 32 for the definition), is not taken into account. The adsorption energy of O in the fcc site (triangle) with a neighboring surface Ag vacancy is also shown for $\theta = 0.25$ ML, as well as the corresponding binding energy.

on the surface, but with increasing coverage the thin (4×4) surface oxide is favored. For higher concentrations, thicker oxide like structures similar to the (111) surface of Ag_2O are preferred which have a coverage of 0.25 ML on the surface and 0.50 ML between each Ag layer. These energetics relate well to the general behavior found experimentally in the early work of Czanderna,[50] whose study shows that the isosteric heat of adsorption of oxygen on silver powder decreases from 0.91 to 0.37 eV per oxygen atom (with respect to 1/2 the binding energy of O_2), and then remains constant at 0.40 ± 0.02 eV per oxygen atom for coverages $\theta = 0.33$ to about 0.90 ML, which was attributed to the growth of an oxide layer.

C. Thermodynamic and kinetic considerations

For a metal in contact with an oxygen atmosphere, in thermal equilibrium, the bulk oxide will be formed when the oxygen chemical potential μ_O satisfies the equation,

$$\mu_O + 2\mu_{Ag(bulk)} = \mu_{Ag_2O}, \tag{4}$$

where $\mu_{Ag(bulk)}$ and μ_{Ag_2O} are the chemical potentials of an Ag atom in bulk and of the bulk oxide Ag_2O, respectively. This equation can be expressed in terms of the total energies of the respective systems, i.e.,

$$E_O + 2E_{Ag} = E_{Ag_2O}. \tag{5}$$

Using the above equation, and referring the energy to that of a free O atom, we obtain for the O chemical potential $\mu_O = 3.23$ eV. This is just the heat of formation of Ag_2O, $\Delta H_{\mathrm{oxide}}$, but referred to a free O atom instead of to $1/2O_2$.

Concerning the transition from chemisorption to bulk oxide formation, it has been proposed that the critical coverage θ_c at which the transition occurs is thermodynamically, rather than kinetically, determined. Below θ_c, the differential heat of adsorption of chemisorbed oxygen is higher than the heat of formation of the oxide, but above θ_c it becomes lower. The differential heat of adsorption at a given coverage $H_{\mathrm{ads}}^{\mathrm{diff}}(\theta)$ can be thought of as the energy required to remove a single O atom on the surface at that coverage, or equivalently, the energy gain on adsorption of a single O atom to result in that coverage (i.e., with the presence of other preadsorbed O atoms). The criteria for the critical coverage beyond which bulk oxide formation is expected to occur is

$$\Delta H_{\text{oxide}} = H_{\text{ads}}^{\text{diff}}(\theta_c) = \left.\frac{d(\theta \times E_{\text{ads}}(\theta))}{d\theta}\right|_{\theta_c}$$

$$= E_{\text{ads}}(\theta_c) + \theta_c \times \left.\frac{dE_{\text{ads}}(\theta)}{d\theta}\right|_{\theta_c}. \quad (6)$$

Applying this to the O/Ag(111) system, using the on-surface adsorption energies from our previous paper,[32] we obtain a critical coverage θ_c of 0.24 ML. This value correlates very closely to the coverage of 0.25 ML found from our extensive DFT calculations when oxygen starts to penetrate into the subsurface region, suggesting onset of oxide formation and occupation of subsurface sites are linked. Similar correlations for O at other transition metal surfaces, namely, Ru(0001), Rh(111), and Pd(111) occur, where it is found that the critical coverage is higher for the ''harder'' metals towards the left of the TM series (i.e., Ru).[21]

In contrast to our theoretical results that predict the formation of oxidelike films, to our knowledge, experimental studies employing high pressures and elevated temperatures have only reported the thin (4×4) surface oxide to date.[29–31,47,51] Formation of an oxide requires first, sufficient numbers of dissociated oxygen atoms, and second, it requires significant mass transport (e.g., diffusion of Ag atoms or O atoms) which can only take place at elevated temperatures. Given that the heat of formation of bulk silver oxide is low, we expect that the formation of thicker oxidelike layers may be prevented either because the temperature at which they are likely to decompose is not high enough for sufficient atomic rearrangements to occur, or that so far there have been insufficient concentrations of oxygen atoms delivered to the surface; indeed the (111) surface of silver has an extremely low dissociative sticking coefficient for O_2, 10^{-6}. Possibly with the use of atomic oxygen or ozone (which readily dissociates at the surface) and low temperatures, thicker oxide films could be formed experimentally. This has recently been done for studies on the oxidation of the Pt(111) surface[52] as well as for polycrystalline silver when exposed at room temperature to a mixture of oxygen and ozone, where thick films have recently been reported.[53]

In order to gain more insight into the behavior of the O/Ag system as an oxidation catalyst and to identify the possibly active O species, it is important to be able to take into account the effect of temperature and gas pressure. In particular, the catalytic reactions of ethylene epoxidation and the partial oxidation of methanol take place at two significantly different temperature ranges (500–600 K and 700–900 K, respectively) and both occur at high (atmospheric) pressure. Our investigations in this direction are in progress.

VI. CONCLUSIONS

In the present work, we have systematically investigated pure subsurface oxygen and structures involving both oxygen adsorbed on the surface and subsurface oxygen, as well as oxidelike structures at the Ag(111) surface through density-functional theory calculations. Compared to pure on-surface oxygen adsorption, which exhibits a strong decrease in adsorption energy with increasing coverage, pure subsurface adsorption exhibits a weak dependence on the coverage, where the octahedral site is favored for all of the investigated coverage range of 0.11 to 1 ML. Comparing the adsorption energies of pure on-surface O and pure subsurface O, we find the former is energetically favored over the latter for coverages up to around 1/2 a monolayer, whereafter the pure subsurface structures are preferred.

The energetically favorable structures involving both on-surface and subsurface oxygen have a lower density of states at the Fermi energy and involve less ionic (less negatively charged) O atoms as compared to the energetically unfavorable structures. As quantified by the concept of a ''removal'' energy, the presence of subsurface oxygen modifies the on-surface oxygen-silver bond significantly. Depending on the adsorption site, it can *either stabilize or destabilize* the on-surface oxygen, and vice versa. The energetically most favorable structures, however, *stabilize* the on-surface oxygen.

On the basis of the energetics of all the calculated structures we find the following scenario: At low coverages oxygen prefers to stay on the surface in the fcc site. With increasing coverage a thin (4×4) surface oxide is energetically favorable, and for higher concentrations, the calculations predict the formation of oxidelike structures very similar to $Ag_2O(111)$. We propose that with the use of atomic oxygen or ozone and low temperatures, such thicker oxidelike films may be observed experimentally.

Having thoroughly studied the energetics, and atomic and electronic properties of the O/Ag(111) system, as is crucial for gaining further understanding into the function of silver as an oxidation catalyst, the next considerations must address the effect of elevated temperatures and high pressures, since these are the conditions, under which the real catalysis takes place. This will be the subject of our following publications.

*Present address: Department of Physics and Astronomy, University of Aarhus, DK-8000 Aarhus, Denmark. Email address: wxli@phys.au.dk

[1] R.A. van Santen and H.P.C.E. Kuipers, Adv. Catal. **35**, 265 (1987), and references therein.

[2] V.I. Bukhtiyarov, M. Hävecker, V.V. Kaichev, A. Knop-Gericke, R.W. Mayer, and R. Schlögl, Catal. Lett. **74**, 121 (2001); Phys. Rev. B (to be published).

[3] R.B. Grant and R.M. Lambert, J. Catal. **92**, 364 (1985).

[4] C. Backx, C.P.M. de Groot, and P. Biloen, Appl. Surf. Sci. **6**, 256 (1980); Surf. Sci. **104**, 300 (1981).

[5] T.E. Felter, W.H. Weinberg, P.A. Zhdan, and G.K. Boreskov, Surf. Sci. **97**, L131 (1980).

[6] I. Wachs and R.J. Madix, Surf. Sci. **76**, 531 (1978).

[7] C. Rehren, M. Muhler, X. Bao, R. Schlögl, and G. Ertl, Z. Phys. Chem. (Munich) **174**, 11 (1991).

[8] W. Segeth, J.H. Wijngaard, and G.A. Sawatzky, Surf. Sci. **194**, 615 (1988).

[9] X. Bao, M. Muhler, Th. Schedel-Niedrig, and R. Schlögl, Phys. Rev. B **54**, 2249 (1996).

[10] D. Herein, A. Nagy, H. Schubert, G. Weinberg, E. Kitzelmann, and R. Schlögl, Z. Phys. Chem. (Munich) **197**, S67 (1996).

[11] X. Bao, G. Lehmpfuhl, G. Weinberg, R. Schlögl, and G. Ertl, J. Chem. Soc., Faraday Trans. **88**, 865 (1992); X. Bao, J.V. Barth, G. Lehmpfuhl, R. Schuster, Y. Uchida, R. Schlögl, and G. Ertl, Surf. Sci. **284**, 14 (1993); X. Bao, M. Muhler, B. Pettinger, R. Schlögl, and G. Ertl, Catal. Lett. **22**, 215 (1993); H. Schubert, U. Tegtmeyer, and R. Schlögl, *ibid.* **28**, 383 (1994); H. Schubert, U. Tegtmeyer, D. Herein, X. Bao, M. Muhler, and R. Schlögl, *ibid.* **33**, 305 (1995).

[12] A. Nagy, G. Mestl, D. Herein, G. Weinberg, E. Kitzelmann, R. Schlögl, J. Catal. **182**, 417 (1999); A. Nagy, G. Mestl, and R. Schlögl, *ibid.* **188**, 58 (1999); A. Nagy and G. Mestl, Appl. Catal., A **188**, 337 (1999).

[13] H. Over, Y.D. Kim, A.P. Seitsonen, S. Wendt, E. Lundgren, M. Schmid, P. Varga, A. Morgante, and G. Ertl, Science **287**, 1474 (2000).

[14] C. Stampfl, M.V. Ganduglia-Pirovano, K. Reuter, and M. Scheffler, Surf. Sci. **500**, 368 (2002).

[15] D. Herein, A. Nagy, H. Schubert, G. Weinberg, E. Kitzelmann, and R. Schlögl, Z. Phys. Chem. (Munich) **197**, 67 (1996).

[16] C. Stampfl, S. Schwegmann, H. Over, M. Scheffler, and G. Ertl, Phys. Rev. Lett. **77**, 3371 (1996).

[17] C. Stampfl, H.J. Kreuzer, S.H. Payne, and M. Scheffler, Appl. Phys. A: Mater. Sci. Process. **69**, 471 (1999).

[18] K. Reuter, M.V. Ganduglia-Pirovano, C. Stampfl, and M. Scheffler, Chem. Phys. Lett. **352**, 311 (2002); Phys. Rev. B **65**, 165403 (2002).

[19] M.V. Ganduglia-Pirovano, K. Reuter, and M. Scheffler, Phys. Rev. B **65**, 245426 (2002).

[20] A.Y. Lozovoi, A. Alavi, and M.W. Finnis, Phys. Rev. Lett. **85**, 610 (2000).

[21] M. Todorova, W.X. Li, M.V. Ganduglia-Pirovano, C. Stampfl, K. Reuter, and M. Scheffler, Phys. Rev. Lett. **89**, 096103 (2002).

[22] A. Kiejna and B.I. Lundqvist, Phys. Rev. B **63**, 085405 (2001); **64**, 049901 (2001).

[23] C. Bungaro, C. Noguera, P. Ballone, and W. Kress, Phys. Rev. Lett. **79**, 4433 (1997).

[24] P. Nordlander and M. Ronay, Phys. Rev. B **36**, 4982 (1987); M. Ronay and P. Nordlander, *ibid.* **35**, 9403 (1987).

[25] G.C. Bond and D.T. Thompson, Catal. Rev. Sci. Eng. **41**, 319 (1999), and references therein.

[26] Y. Uchida, X. Bao, K. Weiss, and R. Schlögl, Surf. Sci. **401**, 469 (1998).

[27] J. Chevrier, L. Huang, P. Zeppenfeld, and G. Comsa, Surf. Sci. **355**, 1 (1996).

[28] Th. Schedel-Niedrig, M. Hävecker, A. Knop-Gericke, and R. Schlögl, Phys. Chem. Chem. Phys. **2**, 3473 (2000).

[29] G, Rovida, F. Pratesi, M. Maglietta, and E. Ferroni, Surf. Sci. **43**, 230 (1974).

[30] C.I. Carlisle, D.A. King, M.L. Bocquet, J. Cerdá, and P. Sautet, Phys. Rev. Lett. **84**, 3899 (2000).

[31] C.I. Carlisle, T. Fujimoto, W.S. Sim, and D.A. King, Surf. Sci. **470**, 15 (2000), and references therein.

[32] W.X. Li, C. Stampfl, and M. Scheffler, Phys. Rev. B **65**, 075407 (2002).

[33] M. Bockstedte, A. Kley, J. Neugebauer, and M. Scheffler, Comput. Phys. Commun. **107**, 187 (1997).

[34] J.P. Perdew, K. Burke, and M. Ernzerhof, Phys. Rev. Lett. **77**, 3865 (1996).

[35] J.A. White and D.M. Bird, Phys. Rev. B **50**, 4954 (1994).

[36] M. Fuchs and M. Scheffler, Comput. Phys. Commun. **116**, 1 (1999).

[37] N. Troullier and J.L. Martins, Phys. Rev. B **43**, 1993 (1991).

[38] J. Neugebauer and M. Scheffler, Phys. Rev. B **46**, 16 067 (1992).

[39] S.L. Cunningham, Phys. Rev. B **10**, 4988 (1974).

[40] M. Scheffler and C. Stampfl, in *Theory of adsorption on metal substrates* edited by K. Horn, M. Scheffler, Handbook of Surface Science, Electronic Structure, Vol. 2.

[41] B. Chakraborty, S. Holloway, and J.K. Nørskov, Surf. Sci. **152-153**, 660 (1985).

[42] L. Pauling, *The Nature of the Chemical Bond* (Cornell University Press, Ithaca, NY, 1960).

[43] M. Rocca, L. Vattuone, L. Savio, F.B. de Mongeot, U. Valbusa, G. Comelli, S. Lizzit, A. Baraldi, G. Paolucci, J.A. Groeneveld, and E.J. Baerends, Phys. Rev. B **63**, 081404 (2001).

[44] M. Taniguchi, K. Tanaka, T. Hashizume, and T. Sakurai, Chem. Phys. Lett. **192**, 117 (1992).

[45] A. Michaelides, A. Alavi, D.A. King, M.-L. Bocquet, and P. Sautet (unpublished)

[46] W.X. Li, C. Stampfl, and M. Scheffler (unpublished).

[47] S. Bare, K. Griffiths, W.N. Lennard, and H.T. Tang, Surf. Sci. **342**, 185 (1995).

[48] B. Pettinger, X. Bao, I.C. Wilcock, M. Muhler, and G. Ertl, Phys. Rev. Lett. **72**, 1561 (1994); B. Pettinger, X. Bao, I. Wilcock, M. Muhler, R. Schlögl and G. Ertl, Angew. Chem. Int. Ed. Engl. **33**, 85 (1994).

[49] A.I. Boronin, V.I. Avdeev, S.V. Koshcheev, K.T. Murzakhmetov, S.F. Ruzankin, and G.M. Zhidomirov, Kinet. Katal. **40**, 721 (1999).

[50] A.W. Czanderna, J. Vac. Sci. Technol. **14**, 408 (1977).

[51] C.T. Campbell, Surf. Sci. **157**, 43 (1985).

[52] N.A. Saliba, Y.-L. Tsai, C. Panja, and B.E. Koel, Surf. Sci. **419**, 79 (1999).

[53] G.I.N. Waterhouse, G.A. Bowmaker, and J.B. Metson, Appl. Surf. Sci. **183**, 191 (2001).